Alexandria Journal of Science and Technology

Article

Optimized Operational Conditions for Removal of Discharged Toxic Silver Nanoparticles from Wastewater using Electrocoagulation

Ghada. E. Abd Elgawad[1], Gehan A. El Naggar[1], Fayza. S. Abdelgeleel[1], Howida. A. Fetouh[2,*]

[1] *Chemistry Department, Faculty of science, Damanhour University, Damanhour 22511, Egypt.*

[2] *Chemistry Department, Faculty of Science, Alexandria University, Alexandria 21321, Egypt.*

**Correspondence Address:*

Howida. A. Fetouh: Chemistry Department, Faculty of Science, Alexandria University, Alexandria, 21321, Egypt. E-mail: howida_fetouh@alexu.edu.eg

KEYWORDS: Electrocoagulation; removal; efficiency; silver nanoparticles; wastewater; treatment.

Received:
July 31, 2023
Accepted:
August 28, 2023
Published:
September 03, 2023

ABSTRACT: Novelty of this study is that it achieved complete removal of toxic silver nanoparticles (AgNPs) using modified electrocoagulation (EC) technology at low energy consumption *via* optimizing operational conditions. It is the first time to explore electrochemical behaviour of anodes materials in EC system. A simple electrolytic cell (DC power source 3V and 200 mA) is used. Aluminium anode is more superior to steel (iron) anode. Percent removal efficiency for both iron and aluminium anodes increased at high current density reached 97% for aluminium at 30 mA cm^{-2} at low energy consumption 3.1 kW h m^{-3} . Supporting electrolyte 10 mL 0.1M NaCl increased solution conductivity and ionic strength. Current efficiency reached 97.2% for 200 ppm AgNPs at optimum operation conditions including current density, electrolysis time, pH and electrodes materials. Designed simple EC reactor at laboratory scale can be scaled up for pilot plant. Redox reactions at electrodes surfaces controlled removal efficiency. Treated effluent was colourless and no AgNPs were detected. Optimized conditions for removal orange colour aqueous solution 200 ppm AgNPs are: Al anode, pencil cathode, pH 4, 2.4V and low current density 30 mA cm^{-2} at agitation speed 50 rotation per min. Efficiency of Al anode is discussed on the basis of electrochemical behaviour using cyclic voltammetry. Electricity consumption decreased by increasing electrolytes conductivity and decreasing anode area.

1. INTRODCTION

Clean water is essential demand: Improved life standard, industry; human, agriculture and energy production. Rapid growing global population face global water scarcity. Global climate changed distribution of fresh water and destabilized water supplies. Declined inadequate water resource and potable water-shortage needs rapid efficient water treatment technologies [1,2]. Municipal sewage discharged into industrial effluents contains storm water sewer and seepage groundwater [3]. Storm water contaminates fresh water. Brackish water and seawater are new norms [4].Water pollutant such as microorganisms, organic matter (OM), heavy metals, ammonia, nutrients and gases (from residential areas, commercial sites, industry, and agriculture, etc.) is a chemical, biological or physical substance decline quality: prevent suitable use, threat living beings causes death millions people [5,6].

Online ISSN: 2974-3273

DOI: 10.21608/AJST.2023.226450.1014

Chemical pollutants are toxic, carcinogenic mutagenic cause teratogenicity [6] impact ecosystem. Undesirable physicochemical and biological properties prevents: domestic, commercial, industrial, agricultural uses and recycling [6].Except distillation, each water treatment technology (reverse osmosis (RO); distillation, freezing, ion exchange, adsorption, neutralization, softening, chemical precipitation, coagulation, disinfection, biological activation and electro dialysis) remove pollutant such as suspended solid, form sludge and biofilm (in presence of N, P, C-nutrients) [7]; cannot remove: toxic NPs and some organics such as surfactants, phenols and pesticides [8, 9].

Electrocoagulation (EC) rapidly simply and safely removes: nutrients, fluorides, persistent chemicals with negligible sludge or secondary pollutions [10]; heavy metals, anions, colorants, oils, suspended solids, pharmaceutical compounds, radioactive elements such as arsenic up to 1ppm [11, 12]; NPs [13, 14]; OM, dyes and silica [10]. Example, removal efficiency (%Re) 98% Cd (II) ions at 1.0 kW h m^{-3}, 20 mA cm^{-2}, pH 7 [15], Table 1.

Table 1. Comparison of EC with some other technologies removed Cd(II) ion [15, 16].

Technology	Filtration	Ion exchange	Adsorption	EC
%Re	86	84	70	98
Reference	27	28	29	26

Energy lose (by over potentials) and consumption limited scale up [16]. Emissions water vapour or ozone results from chemical-, and biological-oxygen demand on drying sludge [17]; Oxides at cathode surface decreases current efficiency; electrodes passivation; Mg-hydroxides inhibited hydrogen evolution reaction and current flow; improper reactor, remained metal ions need removal; replacing consumed anodes [18, 19]; non-destructive AC current and high solution conductivity required. Chlorides from chlorinated compounds require periodical cleaning of electrodes [20].

Toxic AgNPs: harm ecosystem [21]; discharged in rivers, lakes and coastal areas from: domestic gray wastewater from households and institutions [22]; industrial effluents (example: coating, medical devices, electronics, cosmetics, textile and pharmaceutical, medical activity, household food storage, adsorbents, hospitals, environmental and biological areas [21, 22]; dirty wastewater from human activities, food-production& processing); Quantum dots antimicrobial applied in environmental remediation, medicine, pharmaceutical products; biocides; biology; catalysis, optics; bio-; information-technology and security; inkjets; photo-degradation; photography; biosensors and filters [23]; municipal water and post wastewater treatment; release free Ag(I) ions react with ligands in wastewater giving stable toxic Ag complexes and precipitates affect ecosystem and environment; Ag species (interchange into each other, stability depend on ionic strength and OM; inhibits ecological nitrification cycle [23]; lose protective coating agent, aggregate and toxic chemicals decreased metabolism and increases phenols. AgO dissolves give toxic Ag(I) ion [23]; neurotoxic; accumulates in food chain causes environmental and health risks, induce inflammation and memory problems; releases Ag(I) ion at low pH causing oxidative stress and cell damage, alter metabolism by reactive oxygen species; causes weight loss of plants and suppress gene expression and immunity enzymes; damages DNA and reduce productivity.

AgNPs removal by sequencing batch reactor (SBR), sludge bacteria activation, filtration, RO, adsorption (slow need pH adjustment) and ion-exchange showed complexity, high costs and sludge. Expensive adsorbents activated carbon (AC), clays, zeolites, cellulosic materials, graphene and biochar experience pores closure. Adsorbed AgNPs on AC give Ag(I) ions. Micro porous adsorbent rarely recycled, required energy and toxic chemicals for activation and modification and showed interference by other pollutants. Slow coagulation by alum ($Al_2(SO_4)_3$, $FeCl_3$, poly $AlCl_3$ give sludge [24]. Chemical neutralization of these concentrated chemicals form secondary pollutants. Removed by EC using concentrated Na-citrate stabilizer consumed 90 min. at 30 mA cm^{-2} [25]. Reported removal AgNPs by EC are inconsistent and inadequate. This study aims solving problem of potable water shortage by optimizing operational experimental conditions (anode materials; *J*; electrolysis time; pH; initial concentration, Co) for efficient removal using simple EC reactor at minimum energy (by optimizing operation conditions) and no chemicals. Conclusion of this study will discussed in details at the end of the study on expectation that optimizing operation conditions would achieved complete AgNPs removal.

2. Results and Discussion

2.1. Characterization

Figure 1 showed characteristic UV absorption spectra of AgNPs [38].

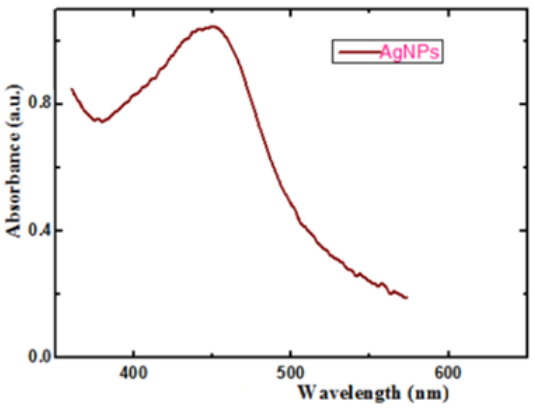

Figure 1. UV-Vis. absorbance band of AgNPs.

Characteristic intense UV-Vis. band at 440 nm is due to electronic transition of surface electrons Plasmon documented for metal nanoparticles with particle size in the range 2-100 nm [26].

Figure 2 showed FTIR spectra of AgNPs and Al and Fe flocs.

Article

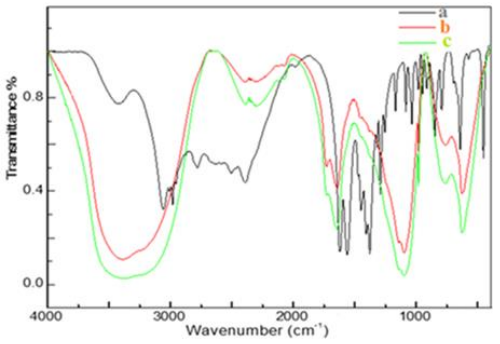

Figure 2. IR spectra: a) AgNPs, b) Fe floc, c) Al floc (*J* 20 mAcm^{-2}, 50 rpm, pH 4, 25ºC, 30 min).

Vibrational IR bands of functional groups assigned as: Intense narrow bands at 3363.80 cm^{-1} to OH stretching O-H hydroxyl groups of Al-, Fe- flocs. More intense bands of Al flocs due to high affinity of Al to oxygen; band at 2984 due to C-H stretching of CH_2 in CMC coating capping agent of AgNPs. Bands of metallic AgNPs at (903.72, 886.32, 666.43, 642.22, 583.30 cm^{-1} are due to stretching vibrations of bonds between Ag^0 and CMC. Intense vibrational bands of stretching Fe-O in $Fe(OH)_3$ at 588 cm^{-1}. Al-and Fe- flocs showed all vibrational bands of AgNPs and metal hydroxides [13, 16, 17]: broad weak intense band at 2050.28, moderate intense band at1534.39, weak bands at (1385.088, 1117.86, 1021.71) and intense bands at 580.06-470.50 [25]. Organic functional groups of CMC gave intense vibrational bands at the frequency range 2000 cm^{-1}-1000 cm^{-1}

TEM micrographs, **Figure 3a** showed spherical mono dispersed AgNPs of particle size smaller than 100 nm. Quantum dot small particles size AgNPs less than 100 nm has high specific surface area and reactivity [27]. **Figure 3 (b,c)** showed SEM micrographs of Fe and Al AgNPs flocs.

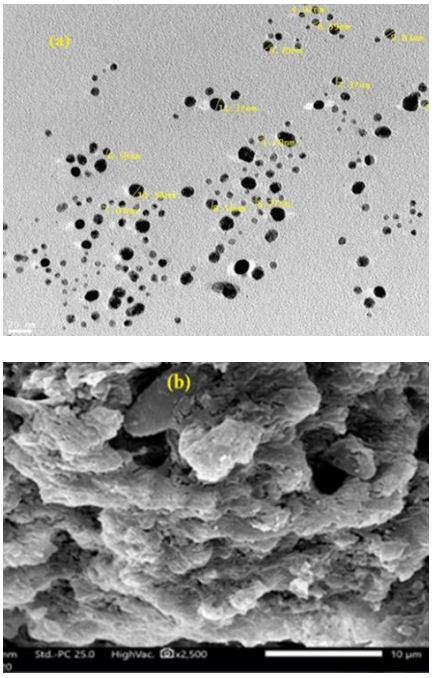

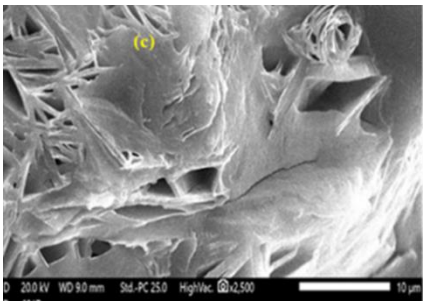

Figure 3 (a-c). SEM micrographs of: a)AgNPs, b) Fe-floc and c) Al-floc respectively ((J 20 mAcm-2, 50. rpm, pH 4, 25oC , 30 min. electrolysis time).

SEM micrographs showed Fe, and Al flocs are massive than AgNPs. The larger µm scale particle size of flocs confirmed AgNPs adsorption on surface of hydroxide $Al(OH)_3$ or $Fe(OH)_3$ [10, 13, 14]. Al-floc is more continuous and denser than Fe-floc indicating preferential adsorption of AgNPs on $Al(OH)_3$ surface.

Figure 4 (a-c) showed pXRD patterns. Characteristic diffractions of AgNPs at 2-thetaº: 37º, 44º, 64º and 74º as intense relatively broad bands indicating long-range order crystallinity and purity [28]. Sharp diffraction peaks of AgNPs followed Bragg law.

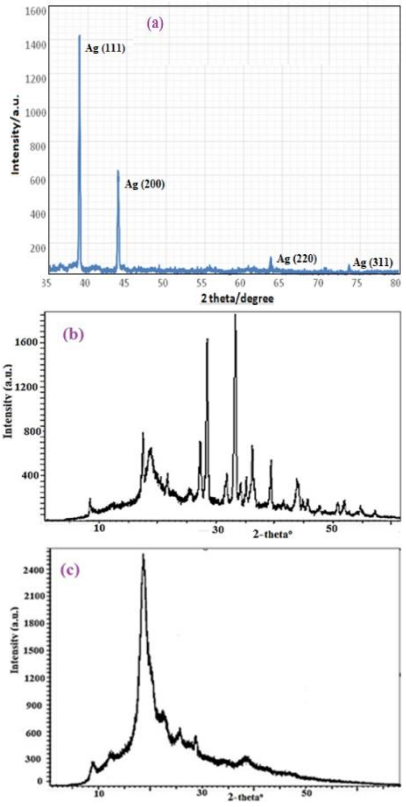

Figure 4 (a-c). pXRD patterns: AgNPs, Fe-AgNPs floc, c)Al-AgNPs floc respectively (*J* 20 mAcm^{-2}, 50 rpm, pH 4, 25ºC, 30 min. electrolysis time).

Lattice planes of samples produce peaks at their corresponding angular positions 2θ obeying Bragg's law. Intense sharp diffraction peaks of AgNPs signifying crystallite size less than 100 nm. AgNPs crystallinity is declined by adsorption on Al(III) and Fe(III) hydroxides. Sharp diffraction peaks of AgNPs replaced by broad diffraction bands in flocs [10]. Peaks of Fe hydroxide appeared at 23° along with diffraction peaks of AgNPs at 2θ°: 38.45°, 46.35°. Disappearance of AgNPs diffraction peak at 64.75° confirmed adsorption on iron hydroxides shell forming flocs. Al floc showed wide continuous diffraction peaks at range 2-theta 9.0°-45°due to incorporated both AgNPs and Al oxide (Al_2O_3) in flocs [14].

2.2. Optimizing experimental conditions for efficient EC

Figure 5 represented triplicates determination of pH effect on *J* mA cm^{-2} on Al and Fe anode, 100 ppm AgNPs, 2.V Volt, 15.0 min. at other fixed parameters.

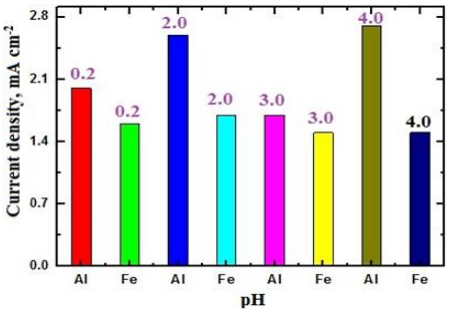

Figure 5. Variation current density on Al and Fe anodes at pH 0.2, 2.0, 3.0 and 4.0 respectively.

Applied 1.1Volts give low residual current for Al and Fe anodes. Large applied potential 2.4V overcame Ohmic and diffusion overvoltages as well as offered activation overvoltages. Al anode showed higher current density *J* than Fe anode at all pH values due to low electrical resistivity and higher activity [29]. The highest *J* of Al at pH 4 indicating increasing numbers of OH^- species that attract Al(III) ion and enhanced formation of Al-hydroxide coagula flocculating AgNPs [30].Current density control effectiveness of EC depending on pH of aqueous solution

pH of the solution adjusted at pH 4 in the following experiments. Al developed thin protective surface Al-oxide film that is quite stable in neutral, acid solutions but attacked by alkali. So high pH is avoided in EC to keep durability of Al anode. Al is a suitable anode and further evaluated in this current study for AgNPs removla. Al has: colorless appearance, nontoxic, good electrical and thermal conductivity and better: reflectivity, lightness and good strength to weight ratio.

Better performance of Al than Fe was confirmed from comparative cyclic voltammetry, **Figure 6** confirmed higher *J* on Al anode than Fe due to: lower charge transfer resistance across Al surface, good redox characteristics and higher chemical equivalent [31].

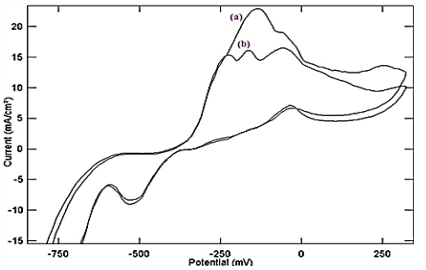

Figure 6. Cyclic voltammogram:a) Al and b) Fe at scan rate 20 mV $min.^{-1}$

This irreversible cyclic voltammograms (CV) indicated non spontaneous anodic axidation of anode surface under applied potential. Al causes higher *J* than Fe for the same applied potential. Anodic oxidation of Fe generates much more hydroxide species (than Al) that retard current flow. *J* increased with increasing the applied potential followed Ohm law of electrolysis [32].

Applied potential (V) = Current flow (I)*Ohmic resistance (R) (1)

Where R includes solution resistance and resistance of external conducting wires.

Figure 7 (a,b) showed, for the same applied potential (1.3V and 1.6V) in 0.1M NaCl at fixed other experimental conditions, current density (*J*) at Al anode is larger than *J* and Fe anode due to better electrical conductivity of Al.

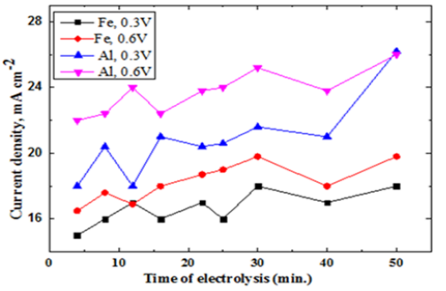

Figure 7. a. Comparative current density on Al anode and Fe anodes.

Fluctuation of current density (*J*) during electrolysis is attributed to electrode polarization by instantaneous accumulation of liberated electrons during anodic oxidation. Al is good anode due to low density, good: mechanical properties, better finishing, corrosion resistance (in acidic and neutral media) and higher electrical conductivity [33].

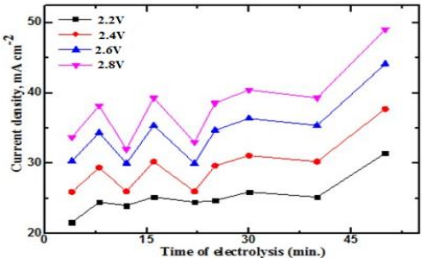

Figure 7. b. Current density of Al anode in 0.1M NaCl at different applied potential.

Applied potential 1.8V give high *J*. However 2.8V was sufficient for metal oxidation giving massive flocs.

Figure 8 showed current density *J* on Al in 100 ppm AgNPs contains 10 mL 0.1 M NaCl increased with decreasing anode surface area from 0.5 cm^2 to 0.1cm^2.

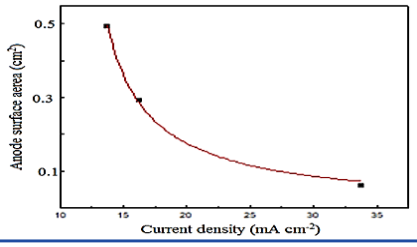

Figure 8. Effect of anode surface area on current density.

NaCl increased ionic conductivity and ionic strength of the solution and facilitated diffusion of AgNPs to the shells of metal hydroxide [13, 34].

Effect of cathode to anode area ratio for Al anode (0.5 cm^2) in 100 mL AgNPs is represented in **Figure 9**. For pencil, Pt. and graphite cathode.

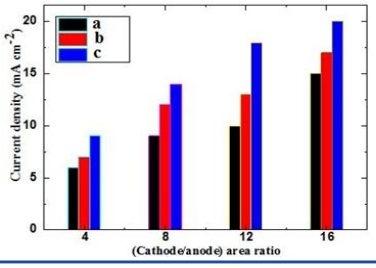

Figure 9. Effect of cathode to anode area ratio and cathode materials (a: graphite, b: Pt, and c: pencil on *J* on Al anode.

At the same operation conditions, as the cathode area increased relative to the anode, *J* increased on anode surface. For the same cathode to anode area ratio, cathode materials increases *J* follows the order:

Pencil > platinum > graphite

Figure 10. Showed EDX analysis of Al before and after immersion in 100 ppm AgNPs at other fixed experimental conditions.

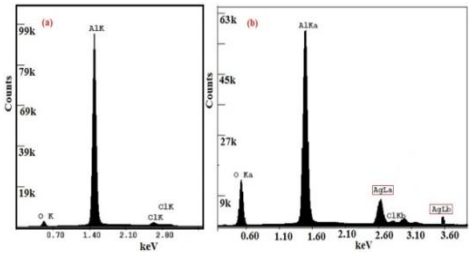

Figure 10. EDX spectra for: a) Al and b) Al floc.

Peaks of O, Al cofirmed formation of Al oxides and hydroxides. Al_2O_3 oxide spontaneously in aerated aqueous solution. Some chloride ions on Al surface from HCl used to adjust pH and NaCl. Atom percent 2.61% Ag are due to adsorded AgNPs. % oxygen is from CMC capping coating agent for AgNPs [35].

2.3. Quantitative analysis

UV-Vis. absorbance bands of AgNPs at 430 nm decreased on passage time of electrolysis, **Figure 11** [42].

Decrease of UV-absorbance of AgNPs due to decrease [AgNPs] by electrocoagulation [36].

At same experimental conditions: Al anode showed higher %Re for AgNPs than Fe. Al anode is effective at low *J* 10, 20 $mAcm^{-2}$. At high *J* 30 mA cm^{-2}, Fe anode is comparable to Al anode, % Re 96.3% and 97.2% respectively due to extensive hydrolysis of large numbers of metal ions. Electrical conductivity of Al and steel are $49.1*10^4$ and $26.0*10^3$ Siemens/cm, respectively. Al had much lower electrical resistivity ($1.506*10^{-5}$ Ohm) than Fe $2.257*10^{-5}$ Ohm [37].

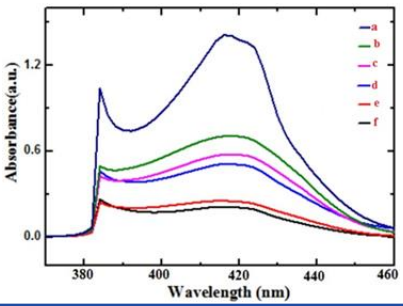

Figure 11. UV-Vis. absorbance bands of AgNPs using Al anode and *J* 20 mA cm^{-2} at electrolysis time (min.): a) 0, b) 10, c) 15, d)20, e)25, f)30.

Table 2 showed %Re AgNPs increased for both iron and Al anodes by increasing *J* at pH 4.0, 50 mL solution, 50 rpm, 500 ppm initial concentration (Co) at 30 min.

Table 2. Effect of current density, J on removal efficiency of 500 ppm AgNPs.

Current density, *J* ($mAcm^{-2}$)	% Re of 500 AgNPs, pH 4, 30 min. time of electrolysis, 1.0V)	
	Fe anode	Al anode
10	40.6	50
20	60.3	86
30	96.3	97.2

Table 3 collected Re for 500 ppm AgNPs by Fe, Al anodes at the fixed operation conditions and 2.4 V at *J* range: 5 mA cm^{-2}-30 mA cm^{-2}.

Table 3. Percent removal 200 ppm AgNPs at different J: Co: 50 rpm, 2.4V using pencil cathode.

Current density, J mA cm^{-2}	%Re AgNPs	
	Fe anode	Al anode
5	63.30	64.10
10	66.60	76.56
15	84.30	87.40
20	87.70	91.00
25	92.20	93.00
30	96.30	97.20

Current density *J* affect adherence of AgNPs on surface of metal hydroxide. At low *J*, migration rate of hydroxyl ion to the region near anode surface is low, Very high *J* avoided as it increase transport rate of ions causing insufficient time for formation Al, Fe hydroxides and decrease coulomb forces between adsorbed AgNPs and shell of metal hydroxide. Optimum *J 30* mA cm^{-2} allowed both diffusion of dissolved ions to away anode/solution interface and moving AgNPs toward shells of metal hydroxides. Mechanical agitation also improved ion diffusion [38].

Higher %Re AgNPs of Al anode than iron anode because Al is an active metal in EMF series, liberates three electrons per atom and has high affinity for oxygen. $Al(OH)_3$ is more thermodynamic stable than $Fe(OH)_3$ [16]. Compared to ferric hydroxide, $Al(OH)_3$ has more residence time for flocculation [39]. Anode in EC-solution had no parasitic reactions (rather than formation of metal ions. Higher %Re AgNPs indicated absence of anode polarization or cathode carbonation that decrease current efficiency [40].

SEM micrographs, **Figure 12** for Al and Fe surface in the same aqueous solution, pH 4 showed different morphology before and after oxidation.

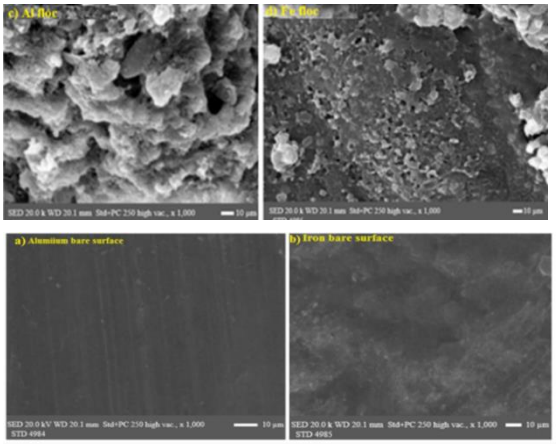

Figure 12. SEM micrographs of: a) Al, b) Fe, c) oxidized Al, d) oxidized Fe (*J* 10 $mAcm^{-2}$, *Co* 500 ppm, 50 rpm, 25°C, pH 4).

Al anode showed more rough and porous surface than Fe anode. Al anode is further evaluated for removal different AgNPs concentrations at low *10* $mAcm^{-2}$ (graphite cathode) Table 4 and **Figure 13**.

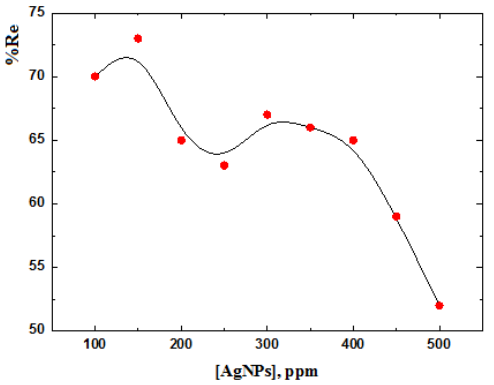

Figure 13. Dependence of %Re of AgNPs on initial concentration.

In this study, removal high AgNPs concentration investigated as high AgNPs concentration is toxic cause lipid peroxidation giving H_2O_2 that penetrates biological cell membranes, interacts with proteins and damage various cellular organelles [41]. High Co increased Ag^0NPs agglomeration by Vander Waals interaction [42]. Irregular %Re at high concentration AgNPs, is due to interference of electrophoresis AgNPs deposited AgNPs on anode surface at concentration above 500 ppm [43].

Table 5 showed comparative removal 500 ppm AgNPs using different cathodes. Low-cost pencil electrode is the most efficient conductive cathode acts by pores and multiple functional groups [44]. Expensive Pt is high conductive but of low porosity. Pencil electrode conducting electricity by extensive delocalized electron density.

Table 4. %Re of different concentrations AgNPs using Al anode at *J* 10 $mAcm^{-2}$.

Concentration, ppm										
Initial, Co	100	150	200	250	300	350	400	450	500	550
Final, C_f	30	41	70	90	100	119	142	186	241	240
Removal efficiency, Re	70	73	65	63	67	66	65	59	52	56

Table 5. Effect of cathode materials on %Re AgNPs using Al anode.

Cathode materials	Pencil	Platinum, Pt	Graphite
Removal efficiency, %Re	80	66	61

2.4. Removal mechanism of AgNPs

In EC, coagulant Fe^{+3} and Al^{+3} ions generated by anodic oxidation of Al and Fe. Hydrolysis of metal ions by hydroxyl ions from water electrolysis giving positively charged metal hydroxides coagulate negatively charged AgNPs by: electrostatic attraction or adsorption. Negatively charged suspended colloidal AgNPs can be neutralized *via* mutual collision with counter ions, (loss net surface charge, electrical double layer (EDL) causing electrostatic repulsion and aggregate by Van der Waal's forces. Flocs separated by skimming and filtration [45]. Yellowish orange color AgNPs is undetected in clear treated water filtrate indicating efficient EC.

$$Fe \rightarrow Fe^{+2} + 2e^{-} \quad (1)$$

$$Fe^{+2} \rightarrow Fe^{+3} + e^{-} \quad (2)$$

Water electrolysis [46]:

$H_2O + 2e^- \rightarrow H^+ + OH^- \rightarrow 2OH^-$ (migrates to anode) $+ H_{2(g)}$ evolved at cathode (3)

pH increase during electrolysis yield different insoluble metal hydroxo complexes such as $Fe(OH)_{2(s)}$ coagulant at pH 5.5-9.5, unimer $Fe(OH)^+$ (pH 9.5-11.4), $Fe(OH)^{-3}$ (pH 11.8-14.0):

$$Fe^{+2} + 2OH \rightarrow FeOH_2 \quad (4)$$

Overall redox reaction: $Fe + 2H_2O \rightarrow Fe(OH)_{2(s)} + H_{2(g)}$ (5)

Ferric hydroxide $Fe(OH)_{3(s)}$ formed at high potential is an effective coagulant.

$$Al \rightarrow Al(III)_{aq.} + 3e^{-} \quad (6)$$

$Al(III)_{aq.}$ yield larger numbers of unimers and polymeric species than steel.

$Al(OH)_3$ is the main coagulant:

Overall reaction: $Al + 3\,H_2O \rightarrow Al(OH)_{3(s)} + 1.5H_{2(g)}$ (7)

The bellow outline structure show illustrated main removal mechanisms AgNPs *via*: adsorption (entrapment charge neutralization by removal electrical double layer around AgNPs and electrostatic attraction between negatively charged AgNPs and positively charged metal hydroxides [46].

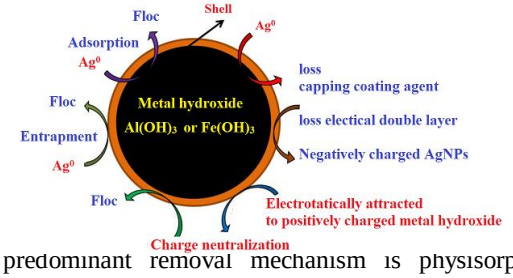

The predominant removal mechanism is physisorption by electrostatic interaction on shell of Fe and Al hydroxides giving flocs as confirmed by FTIR spectra that maintained vibrational bands of CMC capping coating agent of AgNPs.

2.5. Energy consumption

Power density (P, Watt) = electrical current (I) *applied voltage (V) (8)

Energy consumption, E = P*t = I*t/F×V (9)

Where *I*: current (A), *V*: solution volume (m^3), *t*: time (min.), *F:* Faraday's constant 96 500 C mol^{-1}.

Current densities (*J*) 10-20 A m^{-2} correspond to E: 20-30 kW h kg^{-1} for mono-, bi-polar arranged anode; J 20-60 A m^{-2} to 80 kWh kg^{-1} [47].

In this study: E consumed calculated using equation 12, 13 [47]

For $J_{max.}$ 30 mA cm^{-2}:

Current (I, Ampere) = J*anode area= 30*0.1=3 $A.cm^{-2}$ = $3*10^4$ $A.m^{-2}$ (10)

For 30 min. EC operation, I (ampere), time (h), V cubic meter (m^3)

$$E = It/F \times V = \frac{3*10^4*0.5}{96500*50*10^{-6}*10^3} = 3.1 kWh.m^{-3} \quad (11)$$

2.6.Comparative studies to the literature

Microalgae recovery from wastewater at 2.0 kWh·kg^{-1}, 1.1 kWh·kg^{-1} for Fe, Al anodes respectively [48]. Energy harvesting freshwater alga *Chlorella vulgaris* 2.1 kWh/kg reduced to 0.2 kWh/kg under salty conditions for marine alga *Phaeodactylum tricornutum* [49]. Al anodes showed highest harvesting efficiency 95.8% at 0.28 kWh/kg) followed by copper, zinc, and iron [50]. Color removal 100% at 80 min., COD concentration 147 ppm, at 13.56 kWh/L. For durable biochar cathode, 0.0058 kWh/m3 for 90% phosphate removal that was 65% less than that of using carbon cathode [51]. 4.75 KWh/kg were required for removal nitrogen [52]. Energy consumed in our study 3.1kWh.m^{-3} for removal 500 ppm AgNPs with %Re (97.20) and comparable *to E* consumption in removal heavy metal such as Cr(IV) 6.0kWh.m^{-3} [53].

%Re 88%, 93.5%, 98.4% for antibiotics cipro-, levo-, nor floxacin respectively; phosphorus pesticide: %Re 88-96% at 2h, 0.9-3.1 kWh m^{-3}; 85.7%%Re cefazolin at 0.74 kW h kg^{-1} (COD) [28, 29]. Re 91% Cr(IV) ions [54-56].

3. Experimental

3.1. Materials and methods

Synthetic metallic silver Ag^0NPs with zero oxidation state, 99.99% purity coated by carboxy methyl cellulose (CMC); spherical, nm particle size, zeta potential -27.1 mV (stable against aggregation), diffusion coefficient $6.79*10^{-10}$ cm s^{-1}, specific surface area 12 m^2 g^{-1}, density 1.7 g mL^{-1}. Anodes are low-cost commercial carbon steel (Iron) and aluminum (Al) of chemical composition analyzed by source Egyptian Copper Co., Alexandria, Egypt Table 6.

Table 6.Chemical composition of steel and aluminum.

Steel	Element	C	Mn	Si	P	S	Cu	Ni	Cr	V	Fe
	Wt.%	0.37	1.21	0.23	0.02					0.01	0.98
Al	Element	Mn	Ni	Zn	Cu	Ti	Fe	Si	Al		
	Wt.%	0.001				0.003	0.17	0.14	0.997		

Cathodes: Pt. wire 52 mesh particle size, 0.050 inch height, 6 inch width; cheap conductive pencil electrode composite: 56% graphite, 30% clay porous poly Al-silicate (enhanced structural properties (crystal defects, disorder), resin; multi-functional (OH, COOH) graphene oxide decorated by poly oxo metalate; graphite electrode recovered from a medium-sized dry battery. AgNPs and Pt purchased from Sigma Aldrich Co. Al, Fe electrodes from Egyptian Copper Co., Alexandria, Egypt. Pencil electrode obtained from local marketing Library.

Stock solution 1000 ppm AgNPs prepared in double distilled water (to remove interference contaminants). Test solutions 100-600 ppm AgNPs diluted from stock solution. High AgNPs concentrations examined simulated excessive discharged AgNPs in wastewater.

Figure 14 showed Lab. scale EC Plexiglas reactor 50 mL volume capacity and operational conditions. EC conducted at ambient temperature 25ºC and 1.0 atm. pressure. DC current power supply (3.0V and 200 mA). Anode is Al or steel plate (1 cm x1 cm) length and width. Anode surface was carefully step by step polished by using emery papers grades 600, 800 and 1200, washed by: ethanol for 5 min. to remove oxide films or contaminants followed by deionized water (DI), left air drying before EC.

The optimized exposed surface area of anode is 0.1 cm^2. Cathode (Pt. or graphite and pencil electrode) has variable surface area. High cathode to anode area ratio used to maximize *J* on anode surface and minimize energy consumption [57].

Investigated parameters included: Fixed factors (cathode: anode (distance, position and area ratio; temperature 25ºC; solution volume 50 mL and agitation speed 50 rpm) and variable factors (pH; current density *J*; electrode materials; electrolysis time, and initial concentration.

Low concentration 0.1M NaCl improved current flow. pH adjusted using either 0.1MHCl or 0.1M NaOH.,

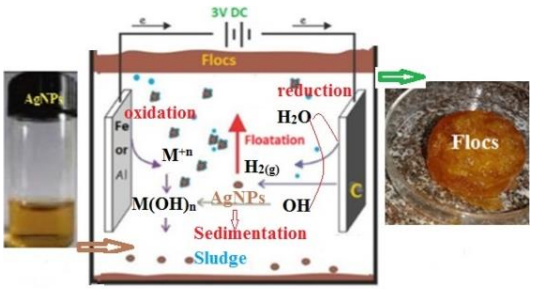

Figure 14. Schematic representation EC and operational parameters.

EC cell operated for specified electrolysis time. Formed floc floated up treated water and removed by skimming. Slight sludge settled down at reactor bottom below clear treated water. EC performed in batch process under specified experimental parameters: ionic strength of solution, pH, applied potential and current density, nature of electrodes materials and initial concentration of AgNPs (Co).

EC system can be scaling up by using heat energy above 300°C from industrial processes, geothermal and nuclear power plants or solar heat, (converted into electricity using thermoelectric solid state generator).

Residual AgNPs after floc sedimentation and filtration in treated wastewater determined using UV-Vis. absorbance spectroscopy at maximum wavelength ($\lambda_{max.}$) 430 nm. Using T70/T80 series UV/Vis. spectrophotometer PG Instrument Ltd., England. Absorbance is converted into concentration by applying Beers Lambert law using calibration curve for a series known concentration. Molar absorptivity coefficient is the slope of straight line of absorbance-concentration plot [35].

$$\% Re = \frac{C_o - C_f}{C_o} \times 100 \quad (12)$$

Where Co, $C_{f:}$ are initial and residual concentration respectively [58].

3.2. Characterizations

AgNPs, brown Fe-hydroxide-AgNPs and white gelatinous Al-hydroxide-AgNPs flocs and anode surfaces characterized using: Fourier Transformer Infrared (FTIR) spectroscopy, Bruker TENSOR 37 spectrophotometer, Model 1430 calibrated by PS film (1602 ±1cm^{-1}) at frequency range 4000-450 cm^{-1}, ambient temperature, sample processed with IR grade dry KBr and pressed into disc pellet; Surface analysis of AgNPs by H-7500 transmission electron TEM microscope (Hitachi, Japan), 20 kV acceleration voltage, sample droplet imaged after air drying on carbon-coated 200-mesh copper grid. Surface morphologies by scanning electron microscope, SEM JSM-IT200; chemical composition; microstructure of Al surface and Al floc by SEM Energy dispersive X-ray (EDS) analysis spectra at 15 kV, Oxford Inca X-act detector; Powder X-ray diffraction (pXRD) patterns at range of incidence-reflection angles 2θ: 5º-70º, 0.02º step, scan rate 1º $min.^{-1}$, 25ºC, Bruker D8 advance XR Germany diffractometer, 40 kV equipped with Cu anticathode Target (Kα Cu illumination radiation, λ 1.54060 Å [59]; Electrical resistivity, ρ of anode sample at 25˚C by two probe method, stable DC power supply and electrometer (Keithley 610). Sample placed between two Cu electrodes and current flow measured as function of applied potential [60]. Electrochemical behavior of Al and Fe anodes in 100 ppm AgNPs investigated by cyclic voltammetry, Gamry Potentiostat USA reference 600, sequencer software version 6.20 setup in three-neck electrochemical cell. Reference electrode (RE): insoluble silver/silver chloride electrode: $Ag/AgCl_{(s)}$, Pt counter electrode (CE) and Al or Fe working electrode (WE) and scan rate 20 mVS^{-1}[61].

4. Conclusion

For the first time low cost electrocoagulation reactor used for complete removal of toxic AgNPs at low energy consumption and low DC potential. %Re 97.2 for 200 ppm AgNPs using Al anode and pencil cathode at low current density 30 mA cm^{-2} and energy consumption 3.1kWh.m^{-3}. Aluminum is: promising efficient anode eco-friendly light metal, abundant, easily recycled, and has high electrical conductivity and low charge transfer resistance; easily formed $Al(OH)_3$ in aqueous solution due to high affinity to hydroxyl ions released from water electrolysis.

Article

AUTHOR INFORMATION

Corresponding Author

Howida. A. Fetouh

Chemistry Department, Faculty of Science, Alexandria University, Alexandria 21321, Egypt

Mail: howida_fetouh@alexu.edu.eg

Mobile: 01203166565

Author Contributions

All authors have given approval to the final version of the manuscript.

Conflicts of interest

Authors have declared no conflict of interest between authors and any producers. The manuscript is advancement of knowledge.

References

[1] He, C., Liu, Z., Wu, J., Pan, X., Fang, Z., Li, J. and Bryan, B.A. Future global urban water scarcity and potential solutions. Nature Communications. 2021, 12(1), 4667.

[2] Vanham, D., Hoekstra, A.Y., Wada, Y., Bouraoui, F., De Roo, A., Mekonnen, M.M., Van De Bund, W.J., Batelaan, O., Pavelic, P., Bastiaanssen, W.G. and Kummu, M. Physical water scarcity metrics for monitoring progress towards SDG target 6.4: An evaluation of indicator 6.4. 2 "Level of water stress". Science of the total environment. 2018, 613, 218-232.

[3] Inyinbor Adejumoke, A., Adebesin Babatunde, O., Oluyori Abimbola, P., Adelani Akande Tabitha, A., Dada Adewumi, O. and Oreofe Toyin, A. Water pollution: effects, prevention, and climatic impact. Water Challenges of an Urbanizing World, Intechopen, China, 2018, 33-47.

[4] Thokchom, B., Qiu, P., Singh, P. and Iyer, P.K. Water Conservation in the Era of Global Climate Change, Elsevier, London, 2021.

[5] Hairom, N.H.H., Soon, C.F., Mohamed, R.M.S.R., Morsin, M., Zainal, N., Nayan, N., Zulkifli, C.Z. and Harun, N.H. A review of nanotechnological applications to detect and control surface water pollution. Environmental Technology & Innovation. 2021, 24, 102032.

[6] Bharagava, R.N., Saxena, G., Mulla, S.I. Introduction to Industrial Wastes Containing Organic and Inorganic Pollutants and Bioremediation Approaches for Environmental Management. In: Saxena, G. and Bharagava, R. eds. Bioremediation of Industrial Waste for Environmental Safety, Singapore: Springer; 2020. p.1-18.

[7] Schweitzer, L. and Noblet, J. Water Contamination and Pollution. In: Török, B. and Dransfield, T. eds. Green Chemistry. London: Elsevier; 2018. p.261-290.

[8] Chen, J., Wu, J., Xu, J., Yuan, Q., Deng, B., Chen, C. and Li, Z. Experiments and insights of desalination by a freezing/thawing method at low subcooling. Chinese Journal of Chemical Engineering. 2020, 28(12), 3011-3017.

[9] Shahzad, M.W., Burhan, M., Ang, L. and Ng, K.C. Energy-water-environment nexus underpinning future desalination sustainability. Desalination. 2017, 413, 52-64.

[10] Jing, G., Ren, S., Pooley, S., Sun, W., Kowalczuk, P.B. and Gao, Z. Electrocoagulation for industrial wastewater treatment: an updated review. Environmental Science: Water Research & Technology. 2021, 7(7), 1177-1196.

[11] Nishad, P.A. and Bhaskarapillai, A. Antimony, a pollutant of emerging concern: A review on industrial sources and remediation technologies. Chemosphere. 2021, 277, 130252.

[12] Pal, P. Treatment and disposal of pharmaceutical wastewater: toward the sustainable strategy. Separation & Purification Reviews. 2018, 47(3), 179-198.

[13] Boinpally, S., Kolla, A., Kainthola, J., Kodali, R. and Vemuri, J.A. state-of-the-art review of the electrocoagulation technology for wastewater treatment. Water Cycle. 2023, 4, 26-36.

[14] Bajpai, M., Katoch, S.S., Kadier, A. and Singh, A.A. Review on electrocoagulation process for the removal of emerging contaminants: theory, fundamentals, and applications. Environmental Science and Pollution Research. 2022, 29(11), 15252-15281.

[15] Alameen, M. and Majeed, N. Removal of cadmium from industrial wastewater using electrocoagulation process. Journal of Engineering. 2020, 26(1), 24-34.

[16] Xu, L., Cao, G., Xu, X., Liu, S., Duan, Z., He, C., Wang, Y. and Huang, Q. Simultaneous removal of cadmium, zinc and manganese using electrocoagulation: Influence of operating parameters and electrolyte nature. Journal of Environmental Management. 2017, 204, 394-403.

[17] Ahangarnokolaei, M.A., Attarian, P., Ayati, B., Ganjidoust, H. and Rizzo, L. Life cycle assessment of sequential and simultaneous combination of electrocoagulation and ozonation for textile wastewater treatment. Journal of Environmental Chemical Engineering. 2021, 9(5), 106251.

[18] Alam, R., Sheob, M., Saeed, B., Khan, S.U., Shirinkar, M., Frontistis, Z., Basheer, F. and Farooqi, I.H. Use of electrocoagulation for treatment of pharmaceutical compounds in water/wastewater: A review exploring opportunities and challenges. Water. 2021, 13(15), 2105.

[19] Moussa, D.T., El-Naas, M.H., Nasser, M. and Al-Marri, M.J.A comprehensive review of electrocoagulation for water treatment: Potentials and challenges. Journal of environmental management. 2017, 186, 24-41.

[20] Sillanpää, M. and Shestakova, M. Electrochemical Water Treatment Methods. In: Sillanpää, M. and Shestakova, M. eds. Electrochemical Water Treatment Methods: Fundamentals, Methods and Full Scale Applications. USA: Butterworth-Heinemann; 2017. p. 47-130.

[21] Ferronato, N. and Torretta, V. Waste mismanagement in developing countries: A review of global issues. International journal of environmental research and public health. 2019, 16(6), 1060.
[22] Manderso, T.M. Overview of existing wastewater management system in case of Debre Markos Town, Ethiopia. Engineering Mathematics. 2018, 2(2), 107.
[23] Fetouh, H.A., Abd-Elnaby, H.M., Alsubaie, M.S. and Sallam, E.R. New experimental low-cost nanoscience technology for formulation of silver nanoparticles-activated carbon composite as a promising antiviral, biocide, and efficient catalyst. Journal of Experimental Nanoscience. 2022, 17(1), 297-314.
[24] Zou, Z., Gu, Y., Yang, W., Liu, M., Han, J. and Zhao, S. A modified coagulation-ultrafiltration process for silver nanoparticles removal and membrane fouling mitigation: The role of laminarin. International Journal of Biological Macromolecules. 2021, 172, 241-249.
[25] Bortoli, L.D., Palácio, S.M., Hermes, E., Zenatti, D.C., Veit, M.T. and Campos, É.A. Removal of silver nanoparticles coated with different stabilizers from aqueous medium by electrocoagulation. Environmental technology. 2018, 41(9), 1139-1150.
[26] Sallam, E.R., Khairy, H.M., Elnouby, M.S. and Fetouh, H.A. Sustainable electricity production from seawater using Spirulina platensis microbial fuel cell catalyzed by silver nanoparticles-activated carbon composite prepared by a new modified photolysis method. Biomass and Bioenergy. 2021, 148, 106038.
[27] Rajan, R., Huo, P., Chandran, K., Dakshinamoorthi, B.M., Yun, S.I. and Liu, B. A review on the toxicity of silver nanoparticles against different biosystems. Chemosphere. 2022, 292, 133397.
[28] Almufarij, R.S., Ali, A.E., Elbah, M.E., Elmaghraby, N.S., Khashaba, M.A., Abdel-Hamid, H. and Fetouh, H.A. Preparation, Characterization of New Antimicrobial Antitumor Hybrid Semi-Organic Single Crystals of Proline Amino Acid Doped by Silver Nanoparticles. Biomedicines. 2023. 11(2), 360.
[29] Sallam, E.R. and Fetouh, H.A. Comparative Study for the Production of Sustainable Electricity from Marine Sediment Using Recyclable Low-Cost Solid Wastes Aluminum Foil and Graphite Anodes. Chemistry Select. 2022, 7(8), e202103972.
[30] Mechelhoff, M., Kelsall, G.H. and Graham, N.J. Electrochemical behaviour of aluminium in electrocoagulation processes. Chemical Engineering Science. 2013, 95, 301-312.
[31] Ru, Y., Zheng, S., Xue, H. and Pang, H. Different positive electrode materials in organic and aqueous systems for aluminium ion batteries. Journal of Materials Chemistry A. 2019, 7(24), 14391-14418.
[32] Ji, X., Hou, S., Wang, P., He, X., Piao, N., Chen, J., Fan, X. and Wang, C. Solid-state electrolyte design for lithium dendrite suppression. Advanced Materials. 2020, 32(46), 2002741.
[33] Modi, M. and Agarwal, G. Effect of aluminium and chromium powder mixed dielectric fluid on electrical discharge machining effectiveness. Advances in Production Engineering & Management. 2019, 14(3), 323–332.
[34] Dires, T.T. and Saroha, A.K. Electrocoagulation: operational parameters, sludge & economic analysis. International Journal of Environmental Analytical Chemistry. 2022, 1-16.
[35] Fetouh, H.A., Abd-El-Nabey, B.A., Goher, Y.M. and Karam, M.S. An electrochemical investigation in the anticorrosive properties of silver nanoparticles for the acidic corrosion of aluminium. Journal of Electrochemistry. 2018, 24(1), 89.
[36] Fetouh, H.A., Hefnawy, A., Attia, A.M. and Ali, E. Facile and low-cost green synthesis of eco-friendly chitosan-silver nanocomposite as novel and promising corrosion inhibitor for mild steel in chilled water circuits. Journal of Molecular Liquids. 2020, 319, 114355.
[37] Kotadia, H.R., Gibbons, G., Das, A. and Howes, P.D. A review of Laser Powder Bed Fusion Additive Manufacturing of aluminium alloys: Microstructure and properties. Additive Manufacturing. 2021, 46, 102155.
[38] Yu, Y., Zhong, Y., Wang, M. and Guo, Z. Electrochemical behavior of aluminium anode in super-gravity field and its application in copper removal from wastewater by electrocoagulation. Chemosphere. 2021, 272, 129614.
[39] Nyangi, M.J., Chebude, Y., Kilulya, K.F. and Salim, C.J. Comparative study on adsorption isotherm and kinetics of defluoridation using aluminum and iron electrodes in electrocoagulation. Chemistry Africa. 2021, 4, 391-398.
[40] Zhu, T., Wang, M., Yu, D., Wang, X., He, A., Yao, G., Xie, C., Tao, L., Guo, Z., Xiao, L. and Chen, J. Improving cathode cleaning and current efficiency by regulating loose scale deposition in scale inhibitor-containing water. Separation and Purification Technology. 2023, 323, 124494.
[41] Plachá, D. and Jampílek, J. Impact of nanoparticles on protozoa. In: Rai, M., Patel, M.and Patel, R. eds. Nanotechnology in Medicine: Toxicity and Safety, USA: John Wiley & Sons Ltd; 2021. p. 67-108.
[42] Wang, J., Sun, Y., Yu, M., Lu, X., Komarneni, S. and Yang, C. Emulsions stabilized by highly hydrophilic TiO2 nanoparticles via van der Waals attraction. Journal of Colloid and Interface Science. 2021, 589, 378-387.
[43] Liu, Q., Ren, J., Lu, Y., Zhang, X., Roddick, F.A., Fan, L., Wang, Y., Yu, H. and Yao, P. A review of the current in-situ fouling control strategies in MBR: Biological versus physicochemical. Journal of Industrial and Engineering Chemistry. 2021, 98, 42-59.
[44] Sreekumar, A., Navaneeth, P., Suneesh, P.V., Nair, B.G. and Babu, T.S. A graphite pencil electrode with electrodeposited Pt-CuO for nonenzymatic amperometric sensing of glucose over a wide linear response range. Microchimica Acta. 2020, 187, 1-8.
[45] Li, K., Zhang, L., Jin, X., Song, J., Jin, P., Wei, Y., Zhu, Y., Liu, M. and Wang, X.C. Removal

performance and membrane fouling mitigation mechanism of electrocoagulation membrane dissolved ozone flotation. Journal of Water Process Engineering. 2021, 43, 102289.

[46] Yasri, N., Hu, J., Kibria, M.G. and Roberts, E.P. Electrocoagulation separation processes. In: Chernyshova, I. eds. Multidisciplinary Advances in Efficient Separation Processes, USA: American Chemical Society; 2020, p. 167-203.

[47] Khan, S.U., Mahtab, M.S. and Farooqi, I.H. Enhanced lead (II) removal with low energy consumption in an electrocoagulation column employing concentric electrodes: Process optimisation by RSM using CCD. International Journal of Environmental Analytical Chemistry. 2021, 1-18.

[48] Parmentier, D., Manhaeghe, D., Baccini, L., Van Meirhaeghe, R., Rousseau, D.P. and Van Hulle, S. A new reactor design for harvesting algae through electrocoagulation-flotation in a continuous mode. Algal Research. 2020, 47, 101828.

[49] Visigalli, S., Barberis, M.G., Turolla, A., Canziani, R., Zrimec, M.B., Reinhardt, R. and Ficara, E. Electrocoagulation–flotation (ECF) for microalgae harvesting–A review. Separation and Purification Technology. 2021, 271, 118684.

[50] Mubarak, M., Shaija, A. and Suchithra, T.V. Flocculation: An effective way to harvest microalgae for biodiesel production. Journal of Environmental Chemical Engineering. 2019, 7(4), 103221.

[51] Bhoi, G.P., Singh, K.S. and Connor, D.A. Optimization of phosphorus recovery using electrochemical struvite precipitation and comparison with iron electrocoagulation system. Water Environment Research. 2023, 95(4), e10847.

[52] Meng, X., Zeng, P., Lin, S., Wu, M., Yang, L., Bao, H., Kang, J., Han, H., Zhang, C. and Sun, W. Deep removal of fluoride from tungsten smelting wastewater by combined chemical coagulation-electrocoagulation treatment: From laboratory test to pilot test. Journal of Cleaner Production. 2023, 416, 137914.

[53] Sharma, D., Pal, D., Athankar, K.K., Prajapati, A.K. and Mehra, S. Removal of chromium (VI) and lead from synthetic solution using electrocoagulation: optimization and performance study. Brazilian Journal of Chemical Engineering.2023, 1-11.

[54] Xu, L., Xu, X., Cao, G., Liu, S., Duan, Z., Song, S., Song, M. and Zhang, M. Optimization and assessment of Fe–electrocoagulation for the removal of potentially toxic metals from real smelting wastewater. Journal of environmental management. 2018, 218, 129-138.

[55] Fang, L., Li, L., Qu, Z., Xu, H., Xu, J. and Yan, N.A novel method for the sequential removal and separation of multiple heavy metals from wastewater. Journal of hazardous materials. 2018, 342, 617-624.

[56] Wu, J., Wang, T., Wang, J., Zhang, Y. and Pan, W.P. A novel modified method for the efficient removal of Pb and Cd from wastewater by biochar: Enhanced the ion exchange and precipitation capacity. Science of the Total Environment. 2021, 754, S142150.

[57] Ingelsson, M., Yasri, N. and Roberts, E.P. Electrode passivation, faradaic efficiency, and performance enhancement strategies in electrocoagulation—a review. Water Research. 2020, 187, 116433.

[58] Batouti, M.E., Sadik, W., Eldemerdash, A.G., Hanafy, E. and Fetouh, H.A.. New and innovative microwave-assisted technology for synthesis of guar gum-grafted acrylamide hydrogel superabsorbent for the removal of acid red 8 dye from industrial wastewater. Polymer Bulletin. 2023, 80(5), 4965-4989.

[59] Liu, Y., Zhang, X., Jiang, W., Wu, M. and Li, Z. Comprehensive review of floc growth and structure using electrocoagulation: Characterization, measurement, and influencing factors. Chemical Engineering Journal. 2021, 417, 129310.

[60] Daskalopoulou, V., Mallios, S., Spanakis-Misirlis, V., Hloupis, G. and Amiridis, V. A low-cost Miniature Field Mill (MiniMill) Electrometer for Atmospheric Electric field Profiling Measurements. 44th COSPAR Scientific Assembly. 2022, Held 16-24 July, 44, 1039.

[61] Gharbi, O., Tran, M.T., Tribollet, B., Turmine, M. and Vivier, V. Revisiting cyclic voltammetry and electrochemical impedance spectroscopy analysis for capacitance measurements. Electrochimica Acta. 2020, 343, 136109.